

AE-PINNS: ATTENTION-ENHANCED PHYSICS-INFORMED NEURAL NETWORKS FOR SOLVING ELLIPTIC INTERFACE PROBLEMS

JIACHUN ZHENG[†], YUNQING HUANG^{‡,*} AND NIANYU YI[§]

ABSTRACT. Inspired by the attention mechanism, we develop an attention-enhanced physics-informed neural networks (AE-PINNs) for solving elliptic interface equations. In AE-PINNs, we decompose the solution into two complementary components: a continuous component and a component with discontinuities across the interface. The continuous component is approximated by a fully connected neural network in the whole domain, while the discontinuous component is approximated by an interface-attention neural network in each subdomain separated by the interface. The interface-attention neural network adopts a network structure similar to the attention mechanism to focus on the interface, with its key extension is to introduce a neural network that transmits interface information. Some numerical experiments have confirmed the effectiveness of the AE-PINNs, demonstrating higher accuracy compared with PINNs, I-PINNs and M-PINNs.

1. INTRODUCTION

The solutions of complex physical problems involve discontinuities caused by multiphysics coupling [1, 2], particularly in interface problems. The interface problems are prevalent in various engineering fields, including materials science [3], fluid dynamics [30], heat transfer [19, 40] and multiphase flow in porous media [4], etc. Classical tailored numerical methods have achieved notable success in solving interface problems, such as the interface-fitted finite element method [5], the immersed interface method [6], the extended finite element method [7] and immersed boundary method [8], the ghost flow method [9], the matched interface and boundary method [10], the discontinuous Galerkin method [11], weak Galerkin method [12], etc.

Based on the universal approximation theorem [13], deep neural networks [14, 15, 16, 17, 18, 19] have introduced novel approaches for developing numerical algorithms to solve PDEs. Unlike classical numerical methods, neural networks provide a nonlinear approximation through diverse network architectures and activation functions in hidden layers. This universal approximation property extends conventional approximation techniques from linear space to nonlinear space. One of the most representative neural network methodologies is physics-informed neural networks (PINNs) [20, 21, 22]. In PINNs framework, the PDEs along with initial and boundary conditions are incorporated into the construction of loss function. By optimizing the loss function through an appropriately chosen optimization algorithm, the optimal network parameters can be obtained. Furthermore, numerous variants of PINNs have been proposed, including gradient-enhanced physics-informed neural networks [23], hp-variational physics-informed neural networks

Key words and phrases. Physics-informed neural networks; Partial differential equations; Attention mechanisms; Elliptic interface problems.

* Corresponding author.

[24], uncertainty quantification physics-informed neural networks with adversarial training [25] and extended physics-informed neural networks (XPINNs) [26] based on domain decomposition.

Although PINNs have been successfully implemented in solving various types of PDEs, including stochastic PDEs [27], fractional-order differential equations [28] and integro-differential equations [29], etc. Problems involving discontinuous solutions have received limited attention. In most neural network architectures for numerical PDEs, activation functions are inherently continuous, making it difficult to accurately capture discontinuities at interfaces. To address these difficulties, several neural network-based methods have been proposed to solve interface problems. In [31], Hu et al. transform interface problems into high-dimensional continuous problems by introducing an additional spatial dimension and then construct a neural network with a single hidden layer to approximate the solution. Additionally, Tseng et al. [32] proposed a novel approach, namely cusp-capturing PINNs, for solving elliptic interface problems. The key idea is to introduce the interface information as additional input into the network. After optimization, the network learns the intrinsic properties of the solution near the interface. In [33], interface PINNs (I-PINNs) were developed to handle interface problems. I-PINNs use neural networks with the same weights and structure in each subdomain, differing only in activation functions. This significantly reduces the number of trainable parameters compared with XPINNs. Li et al. [34] proposed two innovative discontinuity-removing PINNs to solve variable-coefficient elliptic interface problems on curved surfaces. In the Eulerian coordinate framework, surface differential operators are converted into conventional differential operators using level-set functions associated with the surface. And the solution is decomposed into continuous and discontinuous components, each represented by a single neural network that can be trained independently or jointly. A hybrid neural network approach combined with traditional numerical algorithms, termed localized randomized neural networks based on the finite difference method (LRaNN-FDM) [35], has been proposed to solve interface problems. In LRaNN-FDM, a single randomized neural network approximates the solution in each subdomain. Instead of relying on optimization, LRaNN-FDM converts the interface problem into a linear system by using finite difference schemes at randomly sampled points, and then solves the system via least-squares methods.

In this work, we propose an attention-enhanced physics-informed neural networks (AE-PINNs) for solving elliptic interface problems. The key contribution of this work is the proposal of a neural network that integrates interface information, termed the interface-attention neural networks. This model explicitly focuses on the interface by embedding the interface information into the network architecture. In AE-PINNs, the solution is decomposed into continuous and discontinuous components. The discontinuous component is approximated by an interface-attention neural network in each subdomain separated by the interface, while the continuous component is approximated by a fully connected network in the whole domain. Finally, the approximate solution to the interface problem is obtained by combining neural network representations of two components.

The rest of the paper is organized as follows: In section 2, we explain the elliptic interface problems and the AE-PINNs in detail. In section 3, the different elliptic interface problems are

used to test the approximation ability of AE-PINNs. Finally, the advantages and inadequacies of AE-PINNs and its further development are summarized in section 4.

2. ATTENTION-ENHANCED PINNS METHOD FOR INTERFACE PROBLEM

Let $\Omega = \Omega_1 \cup \Omega_2 \cup \Gamma$, where $\Omega \in R^2$, Γ denotes the interface and divides the whole domain Ω into Ω_1 and Ω_2 . \mathbf{n} denotes the normal vector pointing from Ω_1 to Ω_2 along the interface Γ . We consider the following elliptic interface problems:

$$\begin{cases} \nabla \cdot (\alpha(x, y) \nabla u(x, y)) = f(x, y), & (x, y) \in \Omega_1 \cup \Omega_2, \\ ([\alpha \nabla u] \cdot \mathbf{n})(x, y) = \rho(x, y), & (x, y) \in \Gamma, \\ \llbracket u \rrbracket(x, y) = \beta(x, y), & (x, y) \in \Gamma, \\ u(x, y) = h(x, y), & (x, y) \in \partial\Omega, \end{cases} \quad (2.1)$$

where $\llbracket v \rrbracket|_{\Gamma} = v|_{\Omega_1} - v|_{\Omega_2}$ stands for the jump of a function v across the interface Γ , and the diffusion coefficient $\alpha(x, y)$ is piecewise defined

$$\alpha(x, y) = \begin{cases} \alpha_1(x, y), & (x, y) \in \Omega_1, \\ \alpha_2(x, y), & (x, y) \in \Omega_2. \end{cases} \quad (2.2)$$

Note that $u(x, y)$ is continuous in Ω_1 and Ω_2 , respectively, but jumps across the interface Γ :

$$u(x, y) = \begin{cases} u_1(x, y), & (x, y) \in \Omega_1, \\ u_2(x, y), & (x, y) \in \Omega_2. \end{cases} \quad (2.3)$$

When the interface is a closed curve in the computational domain, the solution inside the interface is only constrained by the interface conditions. If the interface conditions are not properly treatment, this will result in a neural network representation with large errors. A natural idea is to integrate interface information into the network structure, this prompts the model to focus more on constraints at the interface.

Since $u(x, y)$ in problem (2.1) is discontinuous at the interface, we can decompose $u(x, y)$ into the following form:

$$u(x, y) = \mu(x, y) + \omega(x, y), \quad (2.4)$$

where $\mu(x, y)$ is continuous over the whole domain, and $\omega(x, y)$ is discontinuous at the interface:

$$\omega(x, y) = \begin{cases} \omega_1(x, y), & (x, y) \in \Omega_1, \\ \omega_2(x, y), & (x, y) \in \Omega_2, \end{cases} \quad (2.5)$$

where $\omega_1(x, y)$ and $\omega_2(x, y)$ are continuous in Ω_1 and Ω_2 respectively.

Based on the expression of $u(x, y)$ in (2.4)-(2.5), we design three networks to represent $\mu(x, y)$, $\omega_1(x, y)$ and $\omega_2(x, y)$, respectively. Noting that $\omega(x, y)$ exhibits discontinuity across the interface, we introduce an interface attention neural network module and design dedicated networks to represent $\omega_1(x, y)$ and $\omega_2(x, y)$.

The attention mechanism [38, 39] is widely used in natural language processing and computer vision. This mechanism mimics the human ability to process external information by filtering out

useless information and focusing on the important information. Based on the attention mechanism, we present a neural network structure with interface information, termed interface-attention neural networks (IA-NNs). The forward propagation rule for IA-NNs with M module is as follows:

$$\begin{aligned}
T(\phi(\mathbf{x})) &= \sigma(W^T \phi(\mathbf{x}) + b^T), \\
H^0 &= \mathbf{x}, \\
Q^n &= W_Q^n H^{n-1} + b_Q^n, \\
K^n &= W_K^n H^{n-1} + b_K^n, \\
V^n &= W_V^n H^{n-1} + b_V^n, \\
Z^n &= \sigma(W^n (\sigma(Q^n \otimes K^n) \otimes V^n) + b^n), \\
H^n &= (1 - Z^n) \otimes T(\Gamma) + Z^n \otimes H^{n-1}, \quad n = 1, 2, \dots, M, \\
u_{IA}(\mathbf{x}, W_{IA}, b_{IA}) &= W^{M+1} H^M + b^{M+1},
\end{aligned} \tag{2.6}$$

where $\mathbf{x} \in R^d$, d is the input dimension, $u_{IA}(\mathbf{x}, W_{IA}, b_{IA})$ is the output of IA-NNs, $\sigma(\cdot)$ denotes the activation function. An adaptive scheme for activation function was proposed in [37] to accelerate convergence in deep and PINNs. \otimes denotes a elementwise multiplication. $T(\phi(\mathbf{x}))$ is a transmitter network that processes, and transmits the interface information, where $\phi(\mathbf{x})$ denotes the level set function derived from the interface, such that $\Gamma = \{\mathbf{x} \in R^d : \phi(\mathbf{x}) = 0\}$. The trainable parameters are given by:

$$\{W_{IA}, b_{IA}\} = \{(W^T, b^T), (W_Q^n, W_K^n, W_V^n, W^n, b_Q^n, b_K^n, b_V^n, b^n)_{n=1}^M, (W^{M+1}, b^{M+1})\}.$$

At first glance, IA-NNs may seem more complex than fully connected neural networks. Note that it is almost same to the attention mechanism, with the addition of a transmitter network $T(\phi(\mathbf{x}))$ and a feature fusion layer H^n . Specifically, the interface information is transmitted into the neural network via a transmitter network, and merged with the internal features in a fully connected layer using a point-wise multiplication. Figure 1(a), (b) show the detailed network structure of the IA-NNs. Figure 1(c) illustrates the AE-PINNs method in detail.

We now construct a AE-PINNs representation of problem (2.1). Firstly, $\mu(x, y)$ in formula (2.4) is approximated by a fully connected neural network, and the expression for a fully connected neural network containing N hidden layers is defined:

$$\begin{aligned}
\Phi^0(\mathbf{x}) &= \mathbf{x}, \\
\Phi^n(\mathbf{x}) &= \sigma(W^n \Phi^{n-1}(\mathbf{x}) + b^n), \quad 1 \leq n \leq N, \\
\mu_{nn}(\mathbf{x}, W, b) &= \Phi^{N+1}(\mathbf{x}) = W^{N+1} \Phi^N(\mathbf{x}) + b^{N+1},
\end{aligned} \tag{2.7}$$

where $W^n \in R^{m_n \times m_{n-1}}$, $b^n \in R^{m_n}$, $\mu_{nn}(\mathbf{x}, W, b)$ is the output of the fully connected neural network and m_{N+1} is the output dimension, $\{W, b\} = \{(W^n, b^n)_{n=1}^{N+1}\}$ denote all the trainable weights and biases. Secondly, $\omega_1(x, y)$ and $\omega_2(x, y)$ in formula (2.5) are approximated by two IA-NNs in (2.6). Thus, an AE-PINNs approximation of an interface problem (2.1) is defined as follows:

$$u_{nn}(x, y, W, b) = \begin{cases} \mu_{nn}(x, y, W_\mu, b_\mu) + u_{IA,1}(x, y, W_1, b_1), & (x, y) \in \Omega_1, \\ \mu_{nn}(x, y, W_\mu, b_\mu) + u_{IA,2}(x, y, W_2, b_2), & (x, y) \in \Omega_2. \end{cases} \tag{2.8}$$

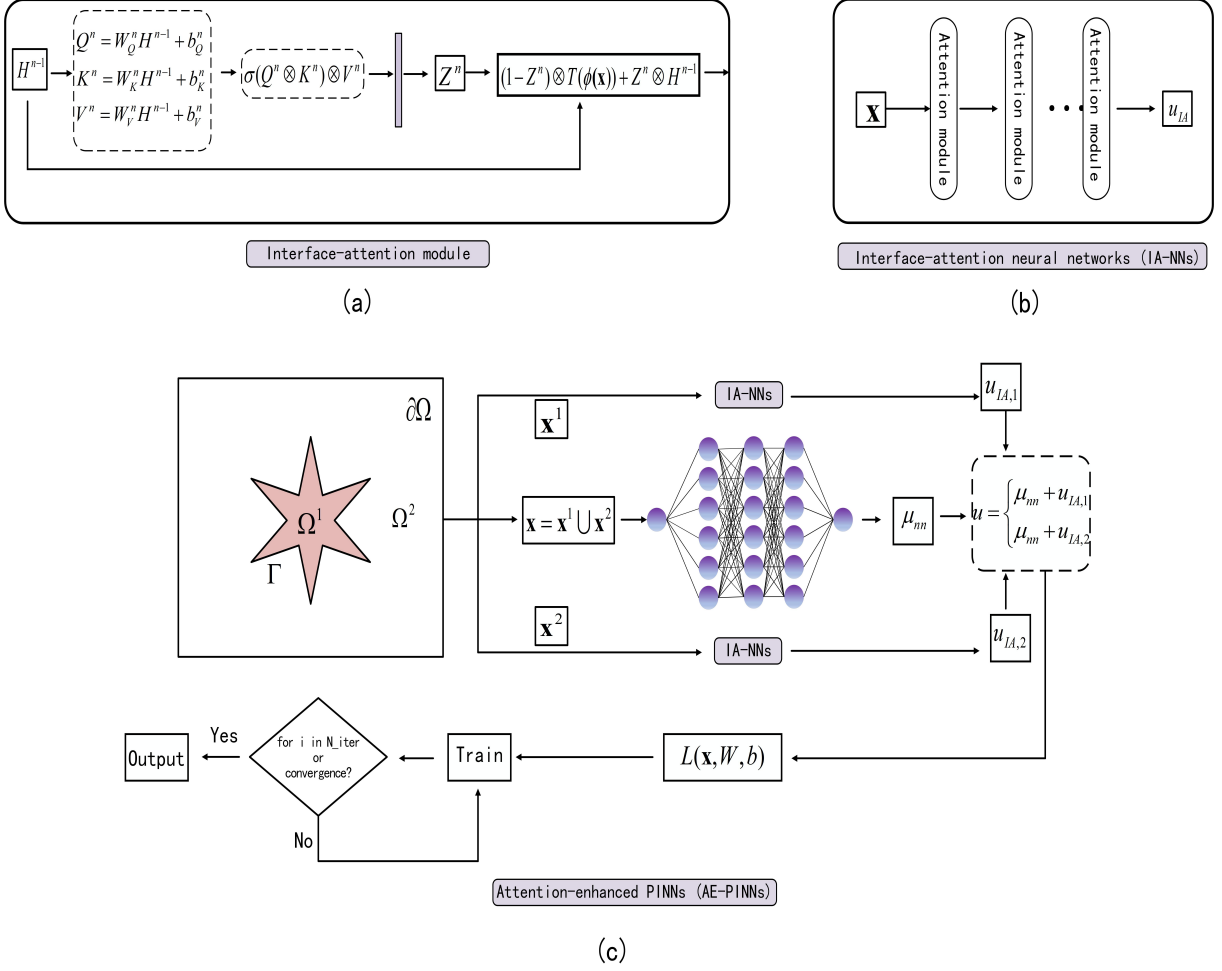


FIGURE 1. (a): interface-attention module, where the gray rectangle represents a fully connected neural network layer. (b): interface-attention neural network (IA-NNs). (c): Attention-enhanced interface PINNs (AE-PINNs).

The interface problem (2.1) is solved by minimizing the loss function $L(x, y, W, b)$:

$$\begin{aligned}
 L(x, y, W, b) = & \tau \frac{1}{N_I} \sum_{i=1}^{N_I} |\nabla(\alpha(x_i, y_i) \nabla u_{nn}(x_i, y_i, W, b)) - f(x_i, y_i)|^2 \\
 & + \tau_b \frac{1}{N_b} \sum_{i=1}^{N_b} |u_{nn}(x_b^i, y_b^i, W, b) - h(x_b^i, y_b^i)|^2 \\
 & + \tau_\Gamma^1 \frac{1}{N_\Gamma^1} \sum_{i=1}^{N_\Gamma^1} |u_{nn}(x_\Gamma^i, y_\Gamma^i, W, b) - \beta(x_\Gamma^i, y_\Gamma^i)|^2 \\
 & + \tau_\Gamma^2 \frac{1}{N_\Gamma^2} \sum_{i=1}^{N_\Gamma^2} |[\alpha(x_\Gamma^i, y_\Gamma^i) u_{nn}(x_\Gamma^i, y_\Gamma^i, W, b)] \cdot \mathbf{n} - \rho(x_\Gamma^i, y_\Gamma^i)|^2,
 \end{aligned} \tag{2.9}$$

where $\{x_i, y_i\}_{i=1}^{N_I}$, $\{x_b^i, y_b^i\}_{i=1}^{N_b}$ and $\{x_\Gamma^i, y_\Gamma^i\}_{i=1}^{N_\Gamma^j}$, $j = 1, 2$ represent the interior points, the boundary points and the interface points, respectively. The parameters $\{\tau, \tau_b, \tau_\Gamma^1, \tau_\Gamma^2\}$ represent the weights

of each component in the $L(x, y, W, b)$. By minimizing the loss function:

$$\{W^*, b^*\} = \arg \min_{\{W, b\}} L(x, y, W, b),$$

we obtain an approximation $u_{nn}(x, y, W^*, b^*)$ of the interface problem (2.1). In order to obtain the optimal parameters $\{W^*, b^*\}$, we use gradient descent method to update the parameters. Concretely, the update rules for step k are as follows:

$$\begin{aligned} W^{k+1} &= W^k - \eta^k \frac{\partial L(x, y, W^k, b^k)}{\partial W^k}, \\ b^{k+1} &= b^k - \eta^k \frac{\partial L(x, y, W^k, b^k)}{\partial b^k}, \end{aligned} \tag{2.10}$$

where η^k denotes the step size of the k -th iteration.

3. NUMERICAL EXPERIMENTS

In this section, we numerically investigate the performance of the proposed AE-PINNs for solving the elliptic interface equations. Figure 1(c) illustrates the AE-PINNs method in detail. For all numerical examples, we set the parameters $\tau = \tau_b = \tau_\Gamma^1 = \tau_\Gamma^2 = 1$, and chose the stochastic gradient descent method (Adam) [41] with a learning rate $\alpha = 0.001$ as the optimizer. Notably, we use 1234 as the global random number seed in all examples. The fully connected neural network is denote by *full-con net* in the parameters list. To better measure the performance of the method, we use the maximum absolute error, the root-mean-square error (RMSE) and the L^2 relative error:

$$\begin{aligned} E_M &= \max_{1 \leq i \leq N_s} |u(\mathbf{x}_i) - u_{nn}(\mathbf{x}_i)|, \\ E_R &= \frac{1}{N_s} \sqrt{\sum_{i=1}^{N_s} |u(\mathbf{x}_i) - u_{nn}(\mathbf{x}_i)|^2}, \\ E_L &= \frac{\sqrt{\sum_{i=1}^{N_s} |u(\mathbf{x}_i) - u_{nn}(\mathbf{x}_i)|^2}}{\sqrt{\sum_{i=1}^{N_s} |u(\mathbf{x}_i)|^2}}. \end{aligned} \tag{3.11}$$

TABLE 1. Comparison of errors in Example 1.

	PINNs	I-PINNs	M-PINNs	AE-PINNs
E_M	2.22×10^{-1}	5.31×10^{-6}	2.87×10^{-6}	1.18×10^{-7}
E_R	1.28×10^{-1}	2.69×10^{-6}	1.35×10^{-6}	3.61×10^{-8}
E_L	1.01	2.10×10^{-5}	1.05×10^{-5}	2.81×10^{-7}

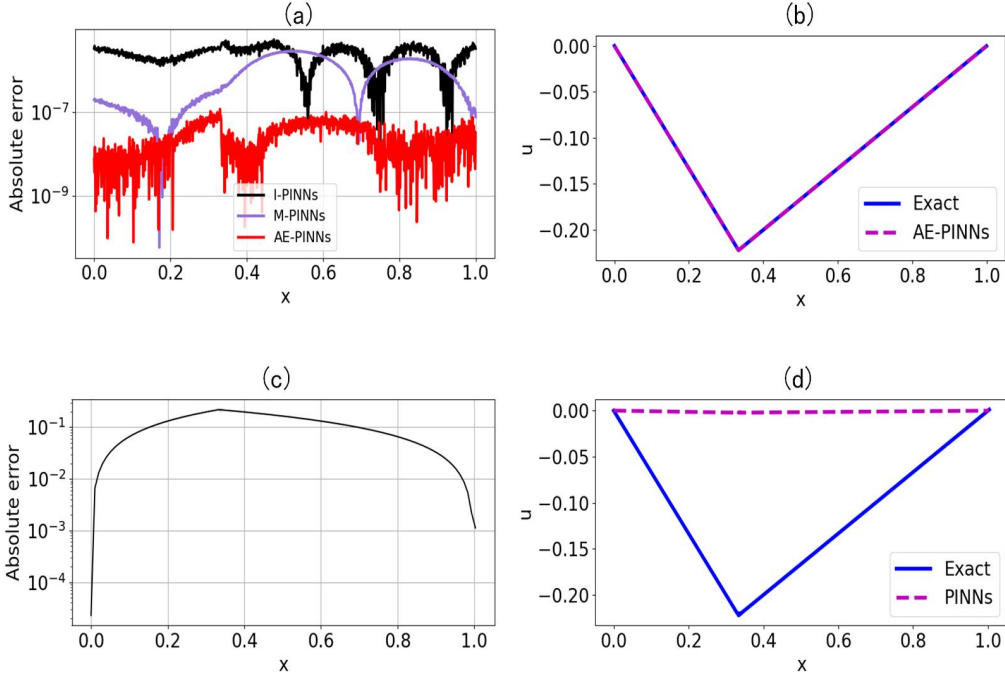


FIGURE 2. Example 1, (a): Absolute errors of M-PINNs, I-PINNs and AE-PINNs. (b): AE-PINNs prediction, exact solution. (c): PINNs absolute errors. (d): PINNs prediction, exact solution.

Example 1. First, we consider the following 1D Poisson equation. The derivative of the exact solution is discontinuous at $x_\Gamma = \frac{1}{3}$:

$$\begin{cases} \Delta u(x) = 0, & x \in (0, 1) \setminus \{x_\Gamma\}, \\ [u](x_\Gamma) = 0, \\ [[\nabla u]](x_\Gamma) = 1, \\ u(0) = u(1) = 0. \end{cases} \quad (3.12)$$

The exact solution:

$$u(x) = \begin{cases} (x_\Gamma - 1)x, & x \in [0, x_\Gamma], \\ x_\Gamma(x - 1), & x \in [x_\Gamma, 1]. \end{cases} \quad (3.13)$$

In this problem, the solution is continuous in the entire domain, but its derivative is discontinuous at $x_\Gamma = \frac{1}{3}$. In order to demonstrate the effectiveness of the proposed algorithm, we choose I-PINNs, multi-domain physics-informed neural networks (M-PINNs) [40] and PINNs as reference algorithms.

The hyperparameters used in the experiments are listed in Table 2. One module with 8 neurons is used for IA-NNs. The level set function derived from the interface is set to $\phi(x) = x - \frac{1}{3}$. A fully connected network with three hidden layers is used to approximate the continuous component. 100 points in the interval $(0, 1)$, two boundary points and one interface point are used for training, and 1000 test points are used to generate network prediction and calculate errors.

Figure 2(a) illustrates the absolute errors of AE-PINNs, I-PINNs and M-PINNs, where the maximum absolute errors of I-PINNs, M-PINNs and AE-PINNs are 5.31×10^{-6} , 2.87×10^{-6} and

1.18×10^{-7} , respectively. Figure 2(b) shows the AE-PINNs approximation and the exact solution, and it can be found that the AE-PINNs accurately approximate the exact solution. Figure 2(c), (d) show the absolute errors of the PINNs, the approximate solution, respectively. Since the activation function is inherently continuous, the PINNs fail to learn the discontinuity of the derivatives at the interface. This results in a prediction of PINNs with large errors.

Table 1 shows the maximum absolute error, the RMSE, and the L^2 relative error for AE-PINNs, I-PINNs and PINNs. By embedding interface information into neural networks, AE-PINNs achieve the best approximation compared with other algorithms. Note that since IA-NNs adopt a network structure similar to the attention mechanism, this may result in a local attention feature similar to the attention mechanism. The neural network representation of the continuous component compensates for this shortcoming. During the experiments, we found that the shallow neural network achieves a good approximation. Therefore, deeper networks are not used in the experiments.

TABLE 2. Parameters of PINNs, I-PINNs, M-PINNs and AE-PINNs in Example 1.

	Hidden layers or IA-NN modules	Neurons	Activation function	Training points /interface points	Iterations
<i>PINNs</i>	3	8	<i>tanh</i>	103/1	20000
<i>I-PINNs</i>					
<i>subnet₁</i>	3	8	<i>sin</i>	52/1	20000
<i>subnet₂</i>	3	8	<i>cos</i>	52/1	20000
<i>M-PINNs</i>					
<i>subnet₁</i>	3	8	<i>sin</i>	52/1	20000
<i>subnet₂</i>	3	8	<i>cos</i>	52/1	20000
<i>AE-PINNs</i>					
<i>full-con net</i>	3	16	<i>tanh</i>	102/0	20000
<i>IA-NN₁</i>	1	8	<i>sin</i>	52/1	20000
<i>IA-NN₂</i>	1	8	<i>cos</i>	52/1	20000

Example 2. We consider a 2D interface problem:

$$\left\{ \begin{array}{ll} \Delta u(x, y) = f(x, y), & (x, y) \in \Omega/\Gamma, \\ u(x, y) = m(x, y), & (x, y) \in \partial\Omega, \\ \llbracket u \rrbracket(x, y) = g(x, y), & (x, y) \in \Gamma, \\ (\llbracket \nabla u \rrbracket \cdot \mathbf{n})(x, y) = h(x, y), & (x, y) \in \Gamma, \end{array} \right. \quad (3.14)$$

where

$$u(x) = \begin{cases} 10^\kappa e^{xy}, & (x, y) \in \Omega_1, \\ 10^{-\kappa} \sin(x) \sin(y), & (x, y) \in \Omega_2. \end{cases} \quad (3.15)$$

TABLE 3. Comparison of errors in Example 2.

	<i>Parameter</i> κ	<i>PINNs</i>	<i>I-PINNs</i>	<i>M-PINNs</i>	<i>AE-PINNs</i>
E_M	2	1.83	3.47×10^{-1}	3.96×10^{-1}	5.46×10^{-3}
	3	4.74	3.63	4.01	1.21×10^{-2}
	4	34.54	37.16	39.67	1.66×10^{-1}
E_R	2	7.36×10^{-1}	2.92×10^{-2}	3.49×10^{-2}	2.17×10^{-3}
	3	9.09×10^{-1}	2.70×10^{-1}	4.76×10^{-1}	1.37×10^{-3}
	4	2.65	2.98	4.16	9.94×10^{-3}
E_L	2	1.96×10^{-2}	7.79×10^{-4}	9.31×10^{-4}	5.79×10^{-5}
	3	2.90×10^{-3}	7.20×10^{-4}	1.26×10^{-3}	3.66×10^{-6}
	4	7.05×10^{-4}	7.95×10^{-4}	1.11×10^{-3}	2.77×10^{-6}

The computational domain $\Omega = [-1, 1]^2$ is divided into two subdomains Ω_1, Ω_2 by the interface Γ , where the interface:

$$\Gamma : r^2(\theta) = x^2 + y^2, \quad r(\theta) = 0.4 + 0.2\sin(20\theta), \quad \theta \in [0, 2\pi].$$

In this case, the level set function derived from the interface is set as follows:

$$\phi(x, y) = \sqrt{x^2 + y^2} - (0.4 + 0.2\sin(20\theta)).$$

Table 4 shows the network parameters of the different neural network algorithms. 500 interior points, 400 boundary points and 120 interface points sampled by the Latin hypercube sampling (LHS) [42] are used for network training. We use 40,000 test points to generate neural network predictions and calculate errors for reference algorithms. During the experiments, two modules are used to construct the IA-NNs, and we use a fully connected network with three hidden layers to approximate the continuous component.

Figure 3 shows the absolute errors (the parameters $\kappa = 2, 3, 4$) of the four neural network algorithms, the results show that AE-PINNs accurately approximate the solution of problem (3.14) compared with other algorithms. Table 3 shows the various errors obtained by the four neural network algorithms. It can be seen that the various error of AE-PINNs is two orders of magnitude lower than that of other algorithms. In subdomain Ω_1 , the solution is only constrained by the interface conditions and multiple components in the loss function interact. A good neural network representation is obtained depending on the interface conditions being sufficiently optimized. By embedding interface information into the network structure, AE-PINNs achieve a better approximation compared with PINNs, I-PINNs and M-PINNs.

TABLE 4. Parameters of PINNs, I-PINNs, M-PINNs and AE-PINNs in Example 2.

	<i>Hidden layers or IA-NN modules</i>	<i>Neurons</i>	<i>Activation function</i>	<i>Training points /interface points</i>	<i>Iterations</i>
<i>PINNs</i>	3	16	<i>tanh</i>	1020/120	50000
<i>I-PINNs</i>					
<i>subnet₁</i>	3	16	<i>sin</i>	320/120	50000
<i>subnet₂</i>	3	16	<i>tanh</i>	820/120	50000
<i>M-PINNs</i>					
<i>subnet₁</i>	3	16	<i>sin</i>	320/120	50000
<i>subnet₂</i>	3	16	<i>tanh</i>	820/120	50000
<i>AE-PINNs</i>					
<i>full-con net</i>	3	16	<i>tanh</i>	900/0	50000
<i>IA-NN₁</i>	2	16	<i>cos</i>	320/120	50000
<i>IA-NN₂</i>	2	16	<i>sin</i>	820/120	50000

Example 3. Next, considering a 2D interface problem with a star-shaped interface:

$$\begin{cases} \nabla(\alpha(x, y)(\nabla u(x, y))), & (x, y) \in \Omega/\Gamma, \\ \llbracket u \rrbracket(x, y) = g(x, y), & (x, y) \in \Gamma, \\ u(x, y) = m(x, y), & (x, y) \in \partial\Omega, \\ (\llbracket \nabla u \rrbracket \cdot \mathbf{n})(x, y) = h(x, y), & (x, y) \in \Gamma. \end{cases} \quad (3.16)$$

The interface is described by a star curve:

$$\Gamma = \{(x, y) : \phi(x, y) = 0, \phi(x, y) = \sqrt{(x^2 + y^2)} - r_0(1 + \sum_{k=1}^3 \beta_k \cos(\eta_k(\arctan(\frac{y}{x}) - \theta_k))\}, \quad (3.17)$$

where the parameters are as follows:

$$\begin{aligned} \beta_1 &= 0.3, & \eta_1 &= 3, & \theta_1 &= 0.5, \\ \beta_2 &= -0.1, & \eta_2 &= 4, & \theta_2 &= 1.8, \\ \beta_3 &= 0.15, & \eta_3 &= 7, & \theta_3 &= 0, & r_0 &= 0.483. \end{aligned} \quad (3.18)$$

The exact solution:

$$u(x, y) = \begin{cases} x^2 + y^2, & (x, y) \in \Omega_1, \\ 0.1(x^2 + y^2)^2 - 0.01 \log(2\sqrt{x^2 + y^2}), & (x, y) \in \Omega_2, \end{cases} \quad (3.19)$$

and

$$\alpha(x, y) = \begin{cases} 4, & (x, y) \in \Omega_1, \\ 10, & (x, y) \in \Omega_2. \end{cases} \quad (3.20)$$

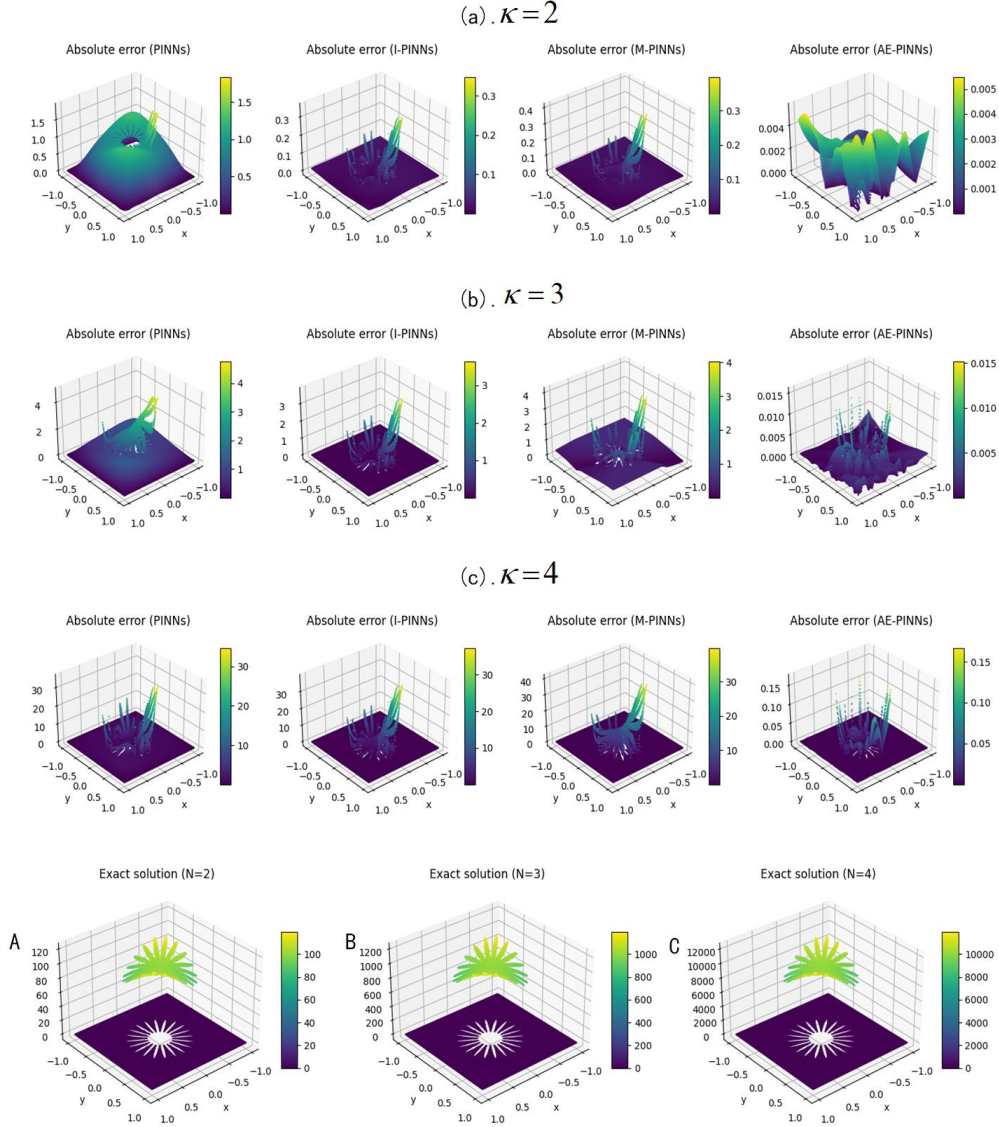


FIGURE 3. Example 2, (**Rows a, b, c**): PINNs, I-PINNs, M-PINNs and AE-PINNs absolute errors ($\kappa=2, 3, 4$). (**A**): Exact solution ($\kappa=2$). (**B**): Exact solution ($\kappa=3$). (**C**): Exact solution ($\kappa=4$).

In this test, we use 400 boundary points, 500 interior points and 600 interface points as training points. The number of iterations reached 10^5 . We use two modules with 48 neurons to build IA-NNs to approximate the discontinuous component. A fully connected neural network with three hidden layers is used to approximate the continuous component. Detailed parameters are listed in Table 5.

Figure 4 shows the absolute errors and approximate solutions obtained by different neural network algorithms. Note that the solution jumps across the interface, and the solution in subdomain Ω_1 is constrained only by the interface conditions. A single neural network with continuous activations function fails to capture discontinuities across the interface, which results in a PINNs

approximation with large errors. Although the approximations of I-PINNs and M-PINNs are improved compared with PINNs, the interface conditions are not properly optimized in I-PINNs and M-PINNs, resulting in error propagation to subdomain Ω_1 . AE-PINNs with interface information provide a more accurate approximation compared with I-PINNs and M-PINNs.

Table 6 provides a detailed comparison of errors. The maximum absolute errors of AE-PINNs, I-PINNs and M-PINNs are 3.05×10^{-4} , 6.51×10^{-3} and 4.26×10^{-3} respectively. The L^2 relative error of AE-PINNs is an order of magnitude lower than that of I-PINNs and M-PINNs. By embedding interface information into neural networks, AE-PINNs accurately capture the discontinuities of solution across the interface.

TABLE 5. Parameters of PINNs, I-PINNs, M-PINNs and AE-PINNs in Example 3.

	<i>Hidden layers or IA-NN modules</i>	<i>Neurons</i>	<i>Activation function</i>	<i>Training points /interface points</i>	<i>Iterations</i>
<i>PINNs</i>	3	48	<i>tanh</i>	1500/600	100000
<i>I-PINNs</i>					
<i>subnet</i> ₁	3	48	<i>cos</i>	713/600	100000
<i>subnet</i> ₂	3	48	<i>sin</i>	1387/600	100000
<i>M-PINNs</i>					
<i>subnet</i> ₁	3	48	<i>cos</i>	713/600	100000
<i>subnet</i> ₂	3	48	<i>sin</i>	1387/600	100000
<i>AE-PINNs</i>					
<i>full-con net</i>	3	20	<i>tanh</i>	900/0	100000
<i>IA-NN</i> ₁	2	48	<i>sin</i>	713/600	100000
<i>IA-NN</i> ₂	2	48	<i>cos</i>	1387/600	100000

TABLE 6. Comparison of errors in Example 3.

	<i>PINNs</i>	<i>I-PINNs</i>	<i>M-PINNs</i>	<i>AE-PINNs</i>
E_M	6.85×10^{-1}	6.51×10^{-3}	4.26×10^{-3}	3.05×10^{-4}
E_R	2.99×10^{-1}	2.19×10^{-3}	1.62×10^{-3}	5.17×10^{-5}
E_L	2.48	2.23×10^{-2}	1.34×10^{-2}	4.28×10^{-4}

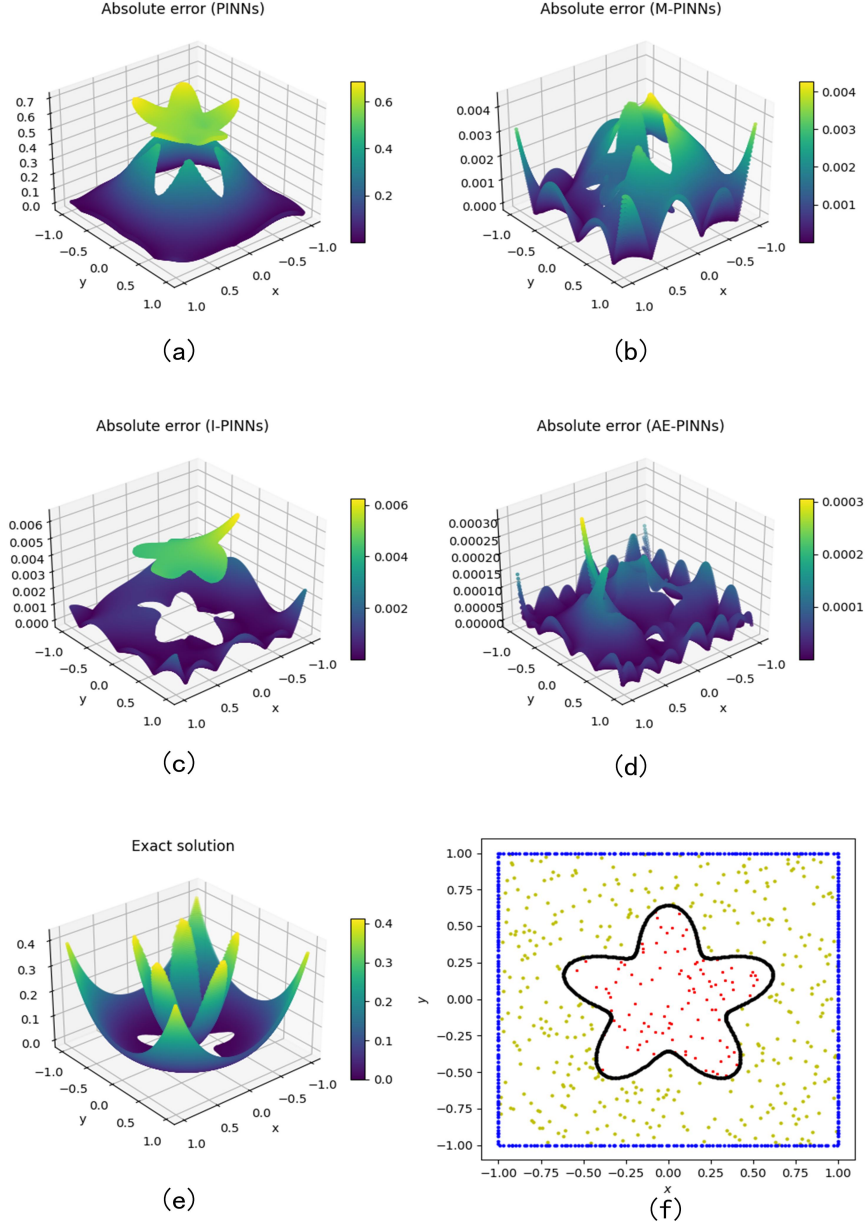


FIGURE 4. Example 3, (a): PINNs absolute error. (b): M-PINNs absolute error. (c): I-PINNs absolute error. (d): AE-PINNs absolute error. (e): Exact solution. (f): Training points.

Example 4. Next, we consider a 3D elliptic interface problem with discontinuous coefficients in the computational domain $\Omega = [-1, 1]^3$.

$$\left\{ \begin{array}{ll} \nabla(\alpha(x, y, z)(\nabla u(x, y, z))) = f(x, y, z), & (x, y, z) \in \Omega/\Gamma, \\ ([\nabla u] \cdot \mathbf{n})(x, y, z) = h(x, y, z), & (x, y, z) \in \Gamma, \\ [u](x, y, z) = g(x, y, z), & (x, y, z) \in \Gamma, \\ u(x, y, z) = m(x, y, z), & (x, y, z) \in \partial\Omega. \end{array} \right. \quad (3.21)$$

An ellipsoidal interface $\Gamma = \{(x, y, z) : \phi(x, y, z) = 0, \phi(x, y, z) = 2x^2 + 3y^2 + 6z^2 - 1.69\}$ divides the domain into non-overlapping subdomains $\Omega_1 = \{(x, y, z) : \phi(x, y, z) \leq 0\}$, $\Omega_2 = \{(x, y, z) : \phi(x, y, z) > 0\}$. The exact solution is piecewise defined:

$$u(x, y, z) = \begin{cases} \sin(2x)\cos(2y)e^z, & (x, y, z) \in \Omega_1, \\ \left(16\left(\frac{y-x}{3}\right)^5 - 20\left(\frac{y-x}{3}\right)^3 + 5\left(\frac{y-x}{3}\right)\right)\log(x+y+3)\cos(z), & (x, y, z) \in \Omega_2. \end{cases} \quad (3.22)$$

The coefficient $\alpha(x, y, z)$ jumps across the interface Γ :

$$\alpha = \begin{cases} 10(1 + 0.2\cos(2\pi(x+y))\sin(2\pi(x-y))\cos(z)), & (x, y, z) \in \Omega_1, \\ 1, & (x, y, z) \in \Omega_2. \end{cases} \quad (3.23)$$

In this test, we use LHS to generate 1500 training points, including 500 interior points, 600 boundary points and 400 interface points. To demonstrate the effectiveness of the proposed method, we use I-PINNs and M-PINNs as reference algorithms. In AE-PINNs, we use a module with 32 neurons to construct the IA-NNs, and the level set function $\phi(x, y, z) = 2x^2 + 3y^2 + 6z^2 - 1.69$. We use a fully connected neural network with three hidden layers to approximate the continuous components. The number of iterations during the training process is set to 50,000. Detailed parameters are listed in Table 7.

This test is similar to Example 2, 3. The solution in subdomain Ω_1 is only constrained by the interface conditions. IA-NNs contain some modules with interface information. These modules are structurally similar to the attention mechanism. IA-NNs explicitly focus on the interface, ensuring that the interface conditions are sufficiently optimized. Figure 5 shows the exact solution of problem (3.21). Figure 6 shows the absolute errors of AE-PINNs, I-PINNs, and M-PINNs at different locations, including interface and boundaries. The results show that the proposed method achieves the best approximation compared with I-PINNs and M-PINNs. Table 8 shows the various errors of the AE-PINNs and the reference methods, including the maximum absolute error, the RMSE, and the L^2 relative error. It can be seen that the errors of AE-PINNs are more than one magnitude lower than those of other algorithms. A series of comparisons demonstrate the effectiveness of AE-PINNs.

Example 5. Finally, we consider a 3D elliptic multiple interface problem. The bubble interface problem in the computational domain $\Omega = [-1, 1]^3$ is used as a test case. The exact solution has the following form:

$$u(x, y, z) = \begin{cases} e^{xyz}, & (x, y, z) \in \Omega_1, \\ 0.1\sin(\pi(x+y))e^{(xyz)}, & (x, y, z) \in \Omega_2, \\ 4x^2 + y^2 + 2z^2, & (x, y, z) \in \Omega_3, \\ e^{x-z}\cos(0.5\pi y), & (x, y, z) \in \Omega_4. \end{cases} \quad (3.24)$$

TABLE 7. Parameters of AE-PINNs, I-PINNs and M-PINNs in Example 4.

	<i>Hidden layers or IA-NN modules</i>	<i>Neurons</i>	<i>Activation function</i>	<i>Training points /interface points</i>	<i>Iterations</i>
<i>I-PINNs</i>					
<i>subnet₁</i>	3	32	<i>sin</i>	620/400	100000
<i>subnet₂</i>	3	32	<i>cos</i>	1280/400	100000
<i>M-PINNs</i>					
<i>subnet₁</i>	3	32	<i>sin</i>	620/400	100000
<i>subnet₂</i>	3	32	<i>cos</i>	1280/400	100000
<i>AE-PINNs</i>					
<i>full-con net</i>	3	20	<i>tanh</i>	1100/0	100000
<i>IA-NN₁</i>	2	32	<i>sin</i>	620/400	100000
<i>IA-NN₂</i>	2	32	<i>cos</i>	1280/400	100000

TABLE 8. Comparison of errors in Example 4.

	<i>I-PINNs</i>	<i>M-PINNs</i>	<i>AE-PINNs</i>
E_M	4.87×10^{-1}	6.77×10^{-1}	2.69×10^{-2}
E_R	1.02×10^{-1}	1.13×10^{-1}	3.98×10^{-3}
E_L	1.64×10^{-1}	1.83×10^{-1}	6.31×10^{-3}

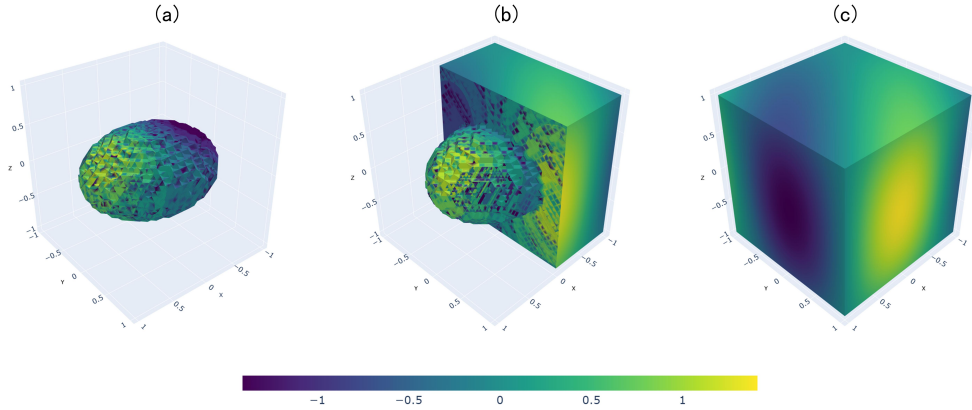


FIGURE 5. Example 4, (a): The exact solution at the interface. (b): The exact solution inside the computational domain. (c): The exact solution at the boundary of the computational domain.

The interfaces are as follows:

$$\begin{aligned}
 \Gamma_1 &= \{(x, y, z) : \phi_1(x, y, z) = 0, \phi_1(x) = (x - 0.25)^2 + (y - 0.25)^2 + z^2 - 0.2^2\}, \\
 \Gamma_2 &= \{(x, y, z) : \phi_2(x, y, z) = 0, \phi_2(x) = (x - 0.5)^2 + (y + 0.25)^2 + z^2 - 0.15^2\}, \\
 \Gamma_3 &= \{(x, y, z) : \phi_3(x, y, z) = 0, \phi_3(x) = x^2 + (y + 0.25)^2 + (z - 0.25)^2 - 0.1^2\}.
 \end{aligned} \tag{3.25}$$

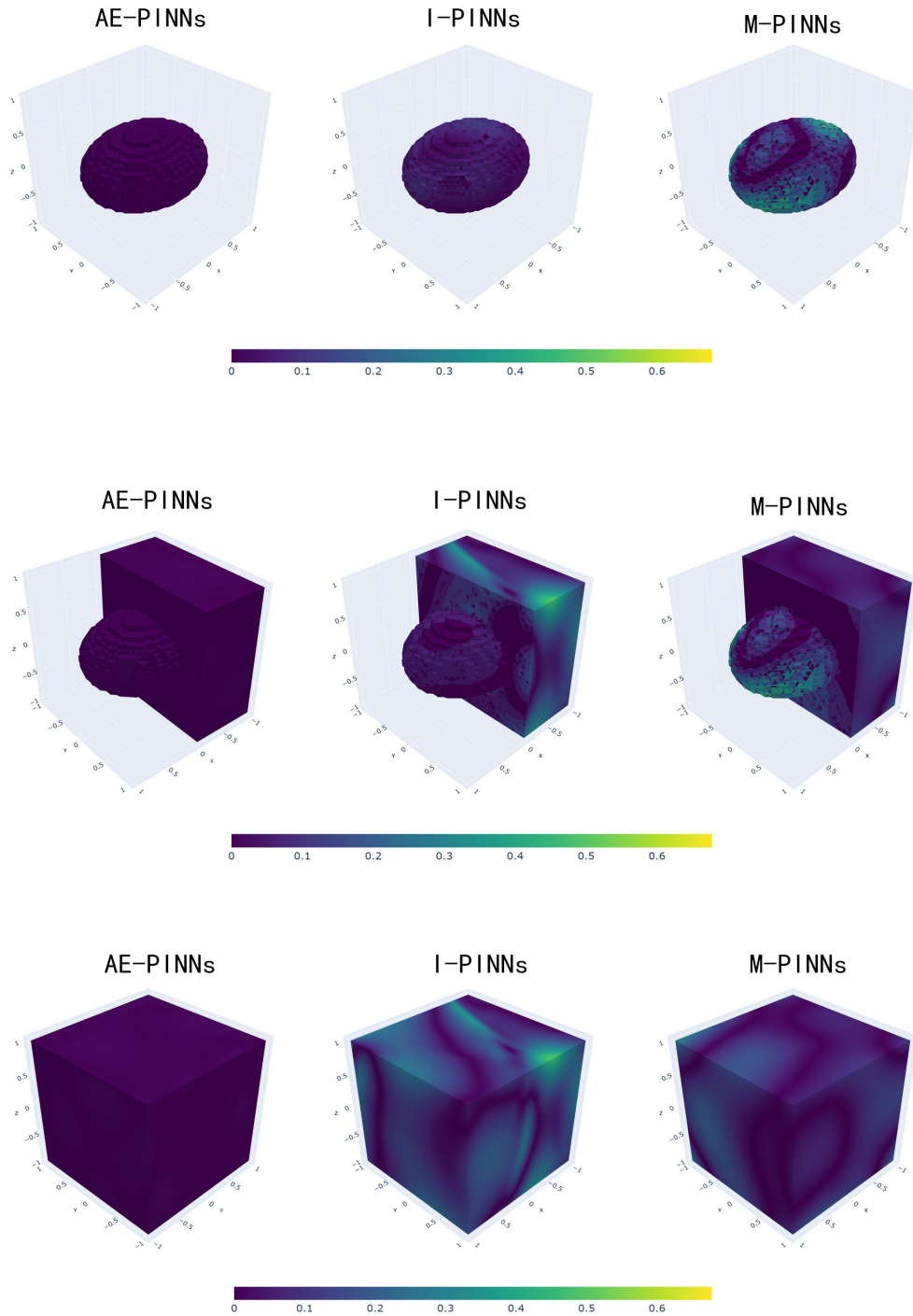


FIGURE 6. Example 4, absolute errors for I-PINNs, M-PINNs, and AE-PINNs. The row-wise captions are; Top: the absolute error at the interface. Middle: the absolute error inside the computational domain. Bottom: the absolute error at the boundary of the computational domain.

In this test, the computational domain is divided into four subdomains by the interfaces. We use a fully connected network with three hidden layers and four IA-NNs, each with one module, to approximate the exact solution. To highlight the performance of the proposed network framework, we choose I-PINNs and M-PINNs as reference algorithms. A total of 2800 training points are used for training, including 1000 interior points, 600 boundary points, and 400 interface points per interface. Table 9 provides a detailed parameter configuration. For the calculation of errors, 100 equally spaced nodes in each dimension (totaling 10^6 test points) are used.

Figure 7 shows the exact solution at different locations. Figure 8 shows the absolute errors obtained by the three neural network algorithms, where the maximum absolute error is 1.01×10^{-2} for AE-PINNs, 1.05×10^{-1} and 3.41×10^{-2} for M-PINNs and I-PINNs, respectively. Table 10 provides a comparison of errors obtained by the three algorithms. Results show that the L^2 relative errors and RMSE obtained by AE-PINNs reach $O(10^{-4})$, while those of I-PINNs and M-PINNs are in the range of $O(10^{-2})$, $O(10^{-3})$, respectively. Combined with the previous examples, it can be seen that the AE-PINNs are sufficiently capable of solving interface problems compared to the I-PINNs and M-PINNs.

TABLE 9. Parameters for AE-PINNs, I-PINNs and M-PINNs in Example 5.

	Hidden layers or IA-NN modules	Neurons	Activation function	Training points /interface points	Iterations
<i>I-PINNs</i>					
<i>subnet</i> ₁	3	32	<i>sigmoid</i>	500/400	50000
<i>subnet</i> ₂	3	32	<i>sin</i>	500/400	50000
<i>subnet</i> ₃	3	16	<i>cos</i>	500/400	50000
<i>subnet</i> ₄	3	16	<i>tanh</i>	2400/1200	50000
<i>M-PINNs</i>					
<i>subnet</i> ₁	3	32	<i>sigmoid</i>	500/400	50000
<i>subnet</i> ₂	3	32	<i>sin</i>	500/400	50000
<i>subnet</i> ₃	3	16	<i>cos</i>	500/400	50000
<i>subnet</i> ₄	3	16	<i>tanh</i>	2400/1200	50000
<i>AE-PINNs</i>					
<i>full-con net</i>	3	16	<i>tanh</i>	1600/0	50000
<i>IA-NN</i> ₁	1	32	<i>cos</i>	500/400	50000
<i>IA-NN</i> ₂	1	32	<i>cos</i>	500/400	50000
<i>IA-NN</i> ₃	1	16	<i>cos</i>	500/400	50000
<i>IA-NN</i> ₄	1	16	<i>sin</i>	2400/1200	50000

TABLE 10. Comparison of errors in Example 5.

	<i>I-PINNs</i>	<i>M-PINNs</i>	<i>AE-PINNs</i>
E_M	1.05×10^{-1}	3.41×10^{-2}	1.01×10^{-2}
E_R	2.24×10^{-2}	2.28×10^{-3}	5.97×10^{-4}
E_L	1.74×10^{-2}	2.21×10^{-3}	4.63×10^{-4}

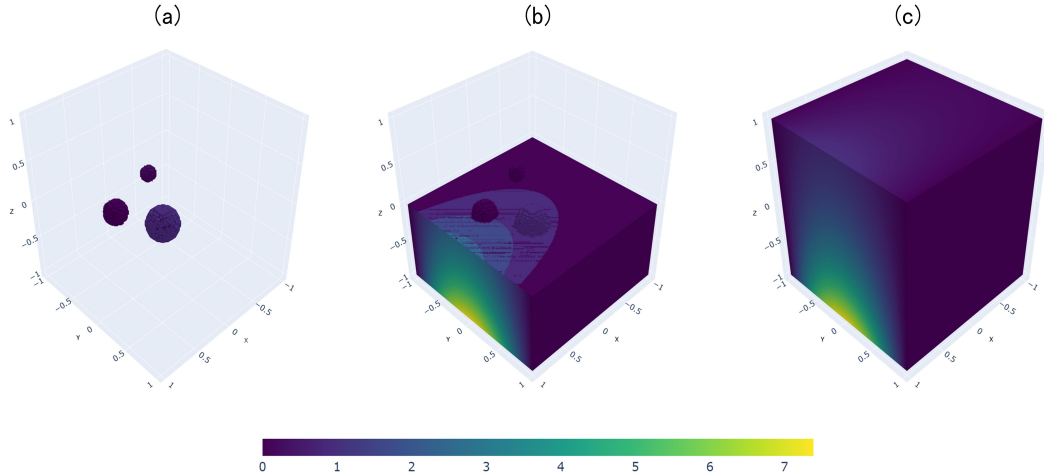


FIGURE 7. Example 5, (a): The exact solution at the interface. (b): The exact solution inside the computational domain. (c): The exact solution at the boundary of the computational domain.

4. SUMMARY AND DISCUSSION

PINNs with continuous activation functions fail to accurately capture the discontinuities of solutions across the interfaces. To alleviate this limitation, we propose an attention-enhanced physics-informed neural networks (AE-PINNs) for solving elliptic interface equations. The proposed algorithm involves the use of domain decomposition and coupling neural networks (we use two neural networks to approximate solution in each subdomain). Concretely, we decompose the solution into two complementary components: a continuous component and a component with discontinuities across the interface. The continuous component is approximated by a fully connected neural network, while the discontinuous component is approximated by IA-NNs with the interface information.

The key contribution of this work is the proposal of interface-attention neural networks (IA-NNs). IA-NNs explicitly focus on the interface, ensuring that the interface conditions are optimized sufficiently during the training process. The performance of four neural network algorithms (PINNs, I-PINNs, M-PINNs and AE-PINNs) for solving interface problems is explored in detail through numerical examples. The results show that the PINNs provide a very bad approximation, which

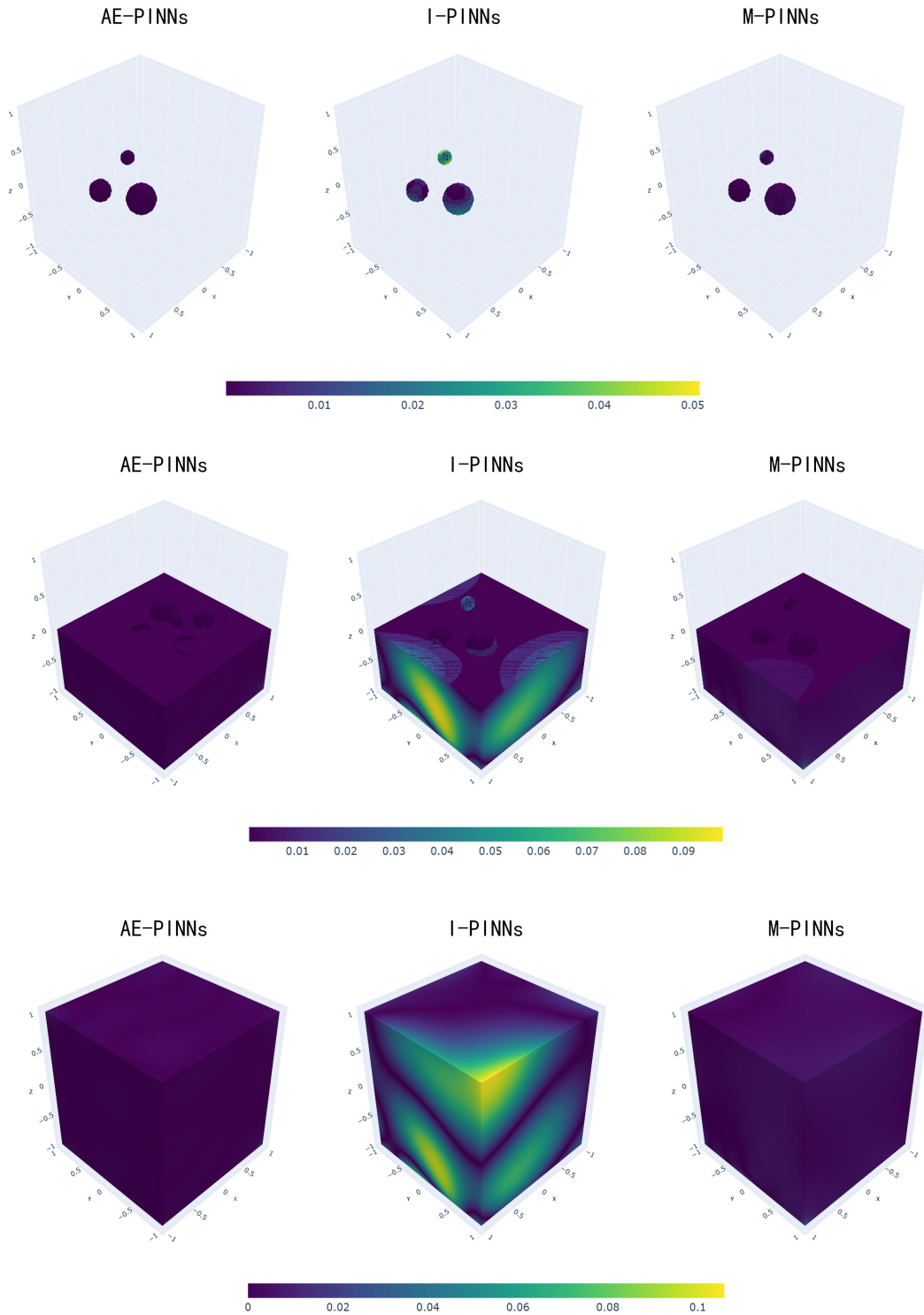


FIGURE 8. Example 5, absolute errors for I-PINNs, M-PINNs and AE-PINNs. The row-wise captions are; Top: the absolute error at the interface. Middle: the absolute error inside the computational domain. Bottom: the absolute error at the boundary of the computational domain.

demonstrates the limitations of the PINNs for solving interface problems. Note that the L^2 relative error of the AE-PINNs is lower than that of the I-PINNs and M-PINNs by at least an order of magnitude for all examples, which demonstrates the effectiveness of the proposed method.

In this work, AE-PINNs result in higher computational cost compared with I-PINNs and M-PINNs. As a future extension of our research, we will focus on developing a simple and efficient network model. In addition, how to embed interface information into the network structure needs to be further discussed.

DECLARATION OF COMPETING INTEREST

The authors declare that they have no known competing financial interests or personal relationships that could have appeared to influence the work reported in this paper.

ACKNOWLEDGMENTS

This work was supported by NSFC Project (12431014) and Project of Scientific Research Fund of the Hunan Provincial Science and Technology Department (2024ZL5017).

REFERENCES

- [1] A. GERSTENBERGER, W.A. WALL, An extended finite element method/Lagrange multiplier based approach for fluid-structure interaction, *Computer Methods in Applied Mechanics and Engineering*, 197 (2008) 1699-1714.
- [2] T.Y. HOU, Z. LI, S. OSHER, H. ZHAO, A hybrid method for moving interface problems with application to the Hele-Shaw flow, *Journal of Computational Physics*, 134 (1997) 236–252.
- [3] D. MEDLIN, G. SNYDER, Interfaces in bulk thermoelectric materials: a review for current opinion in colloid and interface science, *Current Opinion in Colloid & Interface Science*, 14 (4) (2009) 226-235.
- [4] E. HAGHIGHAT, D. AMINI, R. JUANES, Physics-informed neural network simulation of multiphase poroelasticity using stress-split sequential training, *Computer Methods in Applied Mechanics and Engineering*, 397 (2022) 115141.
- [5] J. BRAMBLE, J. KING, A finite element method for interface problems in domains with smooth boundaries and interfaces, *Advances in Computational Mathematics*, 6 (1996) 109-138.
- [6] Z. LI, T. LIN, Y. LIN, R. ROGERS, An immersed finite element space and its approximation capability, *Numerical Methods for Partial Differential Equations*, 20 (2004) 338–367.
- [7] A. HANSBO, P. HANSBO, An unfitted finite element method, based on Nitsche’s method, for elliptic interface problems, *Computer Methods in Applied Mechanics and Engineering*, 191 (2002) 5537-5552.
- [8] C.S. PESKIN, Numerical analysis of blood flow in the heart, *Journal of Computational Physics*, 25 (1977) 220-252.
- [9] X. LIU, T.C. SIDERIS, Convergence of the ghost fluid method for elliptic equations with interfaces, *Mathematics of Computation*, 72 (2003) 1731-1746.
- [10] K. XIA, M. ZHAN, W. GUO, MIB Galerkin method for elliptic interface problems, *Journal of Computational and Applied Mathematics*, 272 (2014) 195-220.
- [11] R. MASSJUNG, An unfitted discontinuous Galerkin method applied to elliptic interface problems, *SIAM Journal on Numerical Analysis*, 50 (2012) 3134-3162.
- [12] L. MU, J. WANG, G. WEI, X. YE, S. ZHAO, Weak Galerkin methods for second order elliptic interface problems, *Journal of Computational Physics*, 250 (2013) 106-125.

- [13] G. CYBENKO, Approximation by superpositions of a sigmoidal function, *Mathematics of Control, Signals and Systems*, 2 (1989) 303-314.
- [14] W. E, B. YU, The deep Ritz method: a deep learning-based numerical algorithm for solving variational problems, *Communications in Mathematics and Statistics*, 6 (2018) 1-12.
- [15] E. KHARAZMI, Z. ZHANG, G.E. KARNIADAKIS, VPINNs: Variational physics-informed neural networks for solving partial differential equations, Preprint at arXiv. abs/1912.00873 (2019).
- [16] Y. KHOO, J. LU, L. YING, Solving for high-dimensional committor functions using artificial neural networks, *Research in the Mathematical Sciences*, 6 (1) (2019) 1-13.
- [17] Y. YANG, M. HOU, J. LUO, Z. TIAN, Numerical solution of several kinds of differential equations using block neural network method with improved extreme learning machine algorithm, *Journal of Intelligent & Fuzzy Systems*, 38 (3) (2019) 3445-3461.
- [18] L. YANG, X. MENG, G.E. KARNIADAKIS, B-PINNs: bayesian physics-informed neural networks for forward and inverse PDE problems with noisy data, *Journal of Computational Physics*, 425 (2020) 109913.
- [19] D. JALILI, S. JANG, M. JADIDI, G. GIUSTINI, A. KESHMIRI, Y. MAHMOUDI, Physics-informed neural networks for heat transfer problems, *International Journal of Heat and Mass Transfer*, 221 (2024) 125089.
- [20] D. ZHANG, L. LU, L. GUO, G.E. KARNIADAKIS, Quantifying total uncertainty in physics-informed neural networks for solving forward and inverse stochastic problems, *Journal of Computational Physics*, 397 (2019) 108850.
- [21] X. MENG, Z. LI, D. ZHANG, G.E. KARNIADAKIS, PPINN: Parareal physics-formed neural network for time-dependent PDEs, *Computer Methods in Applied Mechanics and Engineering*, 370 (2020) 113250.
- [22] A.D. JAGTAP, E. KHARAZMI, G.E. KARNIADAKIS, Conservative physics-informed neural networks on discrete domains for conservation laws, *Computer Methods in Applied Mechanics and Engineering*, 365 (2020) 113028.
- [23] J. YU, L. LU, X. MENG, G.E. KARNIADAKIS, Gradient-enhanced physics-informed neural networks for forward and inverse PDE problems, *Computer Methods in Applied Mechanics and Engineering*, 393 (2022) 114823.
- [24] E. KHARAZMI, Z. ZHANG, G.E. KARNIADAKIS, hp-vpinns: variational physics-informed neural networks with domain decomposition, *Computer Methods in Applied Mechanics and Engineering*, 374 (2021) 113547.
- [25] Y. YANG, P. PERDIKARIS, Adversarial uncertainty quantification in physics-informed neural networks, *Journal of Computational Physics*, 394 (2019) 136-152.
- [26] A.D. JAGTAP, G.E. KARNIADAKI, Extended physics-informed neural networks (XPINNs): A generalized space-time domain decomposition based deep learning framework for nonlinear partial differential equations, *Communications in Computational Physics*, 28 (2020) 2002-2041.
- [27] L. YANG, D. ZHANG, G.E. KARNIADAKIS, Physics-informed generative adversarial networks for stochastic differential equations, *SIAM Journal on Scientific Computing*, 42 (2020) A292-A317.
- [28] G. PANG, L. LU, G.E. KARNIADAKIS, fPINNs: fractional physics-informed neural networks, *SIAM Journal on Scientific Computing*, 41 (2019) A2603-A2626.
- [29] H. ZHANG, X. SHAO, Z. ZHANG, M. HE, E-PINN: extended physics informed neural network for the forward and inverse problems of high-order nonlinear integro-differential equations, *International Journal of Computer Mathematics*, 101 (7) (2024) 723-749.
- [30] X. JIN, S. CAI, H. LI, G.E. KARNIADAKIS, NSF nets (Navier-Stokes flow nets): Physics-informed neural networks for the incompressible Navier-Stokes equations, *Journal of Computational Physics*, 426 (2021) 109951.
- [31] W. HU, T. LIN, M. LAI, A discontinuity capturing shallow neural network for elliptic interface problems, *Journal of Computational Physics*, 469 (2022) 111576.
- [32] Y. TSENG, T. LIN, W. HU, M. LAI, A cusp-capturing PINN for elliptic interface problems, *Journal of Computational Physics*, 491 (2023) 112359.
- [33] A.K. SARMA, S. ROY, C. ANNAVARAPU, P. ROY, S. JAGANNATHAN, Interface PINNs (I-PINNs): A physics-informed neural networks framework for interface problems, *Computer Methods in Applied Mechanics and Engineering*, 429 (2024) 117135.

- [34] H. LI, H. FAN, Z. TAN, Two novel discontinuity-removing PINNs for solving variable coefficient elliptic interface problems on curved surfaces, *Computer Methods in Applied Mechanics and Engineering*, 435 (2025) 117637.
- [35] Y. LI, F. WANG, Local randomized neural networks with finite difference methods for interface problems, *Journal of Computational Physics*, 529 (2025) 113847.
- [36] S. WANG, Y. TENG, P. PERDIKARIS, Understanding and mitigating gradient flow pathologies in physics-informed neural networks, *SIAM Journal on Scientific Computing*, 43 (5) (2021) A3055-A3081.
- [37] A.D. JAGTAP, K. KAWAGUCHI, G.E. KARNIADAKIS, Adaptive activation functions accelerate convergence in deep and physics-informed neural networks, *Journal of Computational Physics*, 404 (2020) 109136.
- [38] A. VASWANI, N. SHAZEER, N. PARMAR, J. USZKOREIT, L. JONES, A. N. GOMEZ, L. KAISER, I. POLOSUKHIN, Attention is all you need, in *Advances in Neural Information Processing Systems*, (2017) 5998-6008.
- [39] X. LIU, H. YU, I. DHILLON, C. HSIEH, Learning to encode position for transformer with continuous dynamical model, *Association for Computing Machinery*, 587 (2020) 6327-6335.
- [40] B. ZHANG, G. WU, Y. GU, X. WANG, F. WANG, Multi-domain physics-informed neural network for solving forward and inverse problems of steady-state heat conduction in multilayer media, *Physics of Fluids*, 34 (2022) 116116.
- [41] D.P. KINGMA, J. BA, Adam: A method for stochastic optimization, *CoRR*, arXiv:1412.6980 (2014).
- [42] M. STEIN, Large sample properties of simulations using Latin hypercube sampling, *Technometrics*, 29 (2) (1987) 143-151.

[‡] SCHOOL OF MATHEMATICS AND COMPUTATIONAL SCIENCE, XIANGTAN UNIVERSITY, XIANGTAN 411105, P.R.CHINA

Email address: jczheng2022@126.com

[‡] NATIONAL CENTER FOR APPLIED MATHEMATICS IN HUNAN, KEY LABORATORY OF INTELLIGENT COMPUTING & INFORMATION PROCESSING OF MINISTRY OF EDUCATION, XIANGTAN UNIVERSITY, XIANGTAN 411105, HUNAN, P.R.CHINA

Email address: huangyq@xtu.edu.cn

[§] HUNAN KEY LABORATORY FOR COMPUTATION AND SIMULATION IN SCIENCE AND ENGINEERING; SCHOOL OF MATHEMATICS AND COMPUTATIONAL SCIENCE, XIANGTAN UNIVERSITY, XIANGTAN 411105, P.R.CHINA

Email address: yiniany@xtu.edu.cn